

Charge-ordered spinel AlV_2O_4 : High-energy-resolution EELS and computational studiesØ. Prytz,¹ E. Flage-Larsen,¹ L. Gu,^{2,3} W. Sigle,² P. A. van Aken,² and J. Taftø¹¹*Department of Physics, University of Oslo, P. O. Box 1048 Blindern, NO-0316 Oslo, Norway*²*Max Planck Institute for Intelligent Systems, Heisenbergstraße 3, D-70569 Stuttgart, Germany*³*Beijing National Laboratory for Condensed Matter Physics, Institute of Physics, Chinese Academy of Science, Beijing 100190, China*

(Received 7 February 2012; revised manuscript received 18 April 2012; published 8 May 2012)

The electronic and magnetic structure of the charge-ordered spinel AlV_2O_4 is studied using a combination of high-energy-resolution electron energy-loss spectroscopy and density functional theory. We find that the vanadium atoms have a fractional valence close to 2.4+ and display a charge and magnetic ordering consistent with previous reports. The oxygen K edge features a prominent prepeak indicative of a strong hybridization of O $2p$ and V $3d$ hole states. Experiments at high temperatures confirm a structural transition to a non-charge-ordered state, although no effects of this are observed in the spectra.

DOI: [10.1103/PhysRevB.85.195112](https://doi.org/10.1103/PhysRevB.85.195112)

PACS number(s): 79.20.Uv, 71.20.-b, 71.27.+a

I. INTRODUCTION

In transition metal oxides, the electron-electron interaction may be central to understanding the materials properties. The strong electron correlation may cause the electrons to be partially localized, and strong couplings between spin, charge, and orbital degrees of freedom can give rise to properties such as high-temperature superconductivity, metal-insulator transitions, and colossal magnetoresistance. In order to tailor these functional properties, a detailed understanding of their origins at the atomic scale is needed. To this end, experimental studies of the electronic structure using photoemission spectroscopy or electron energy-loss spectroscopy can provide invaluable contributions,¹⁻³ in particular when combined with electronic structure calculations from first principles.^{4,5}

At high temperature, AlV_2O_4 is a cubic spinel with Al on the tetrahedral sites and V on the octahedral sites. At approximately 700 K, there is a structural phase transition to a lower-symmetry trigonal structure.⁶ In 2003, Matsuno and co-workers reported that this phase transition was accompanied by “anomalies” in both resistivity and magnetic susceptibility.⁷ Taken together with electron diffraction experiments, they concluded that the compound enters a charge-ordered state, where vanadium atoms of different valencies occupy distinct crystallographic sites and are stacked along the cubic [111] axis. The crystal structure has since been further refined,⁶ the effect of doping with Cr has been studied,^{7,8} and theoretical studies have been performed.^{9,10}

However, there has to our knowledge been no direct experimental investigation of the electronic structure and bonding of this system. Here, we perform electron energy-loss spectroscopy (EELS) in a transmission electron microscope (TEM) to study the bonding characteristics of the charge-ordered AlV_2O_4 . Performing such experiments in a TEM offers the benefit of obtaining the electronic structure of the material while simultaneously observing the crystal structure and chemical composition. These investigations are combined with calculations of the electronic structure using density functional theory (DFT) and real-space multiple-scattering (RSMS) techniques. We experimentally obtain the average valence of vanadium and show a high degree of agreement between the experimentally obtained spectra and the theoretically calculated density of states.

II. EXPERIMENTAL AND THEORETICAL TECHNIQUES**A. Sample synthesis and specimen preparation**

Samples were prepared by reaction of Al, V_2O_3 , and V_2O_5 powders in a sealed and evacuated silica ampoule at 1100 °C for 150 h.⁷ The resulting powder was analyzed by x-ray diffraction, revealing only small amounts of impurity phases in addition to the low-temperature AlV_2O_4 phase. Samples for transmission electron microscopy were prepared by crushing in ethanol and deposited on a carbon film suspended on a copper grid. The composition and structure of each single crystal used for the EELS studies were checked by energy-dispersive x-ray spectroscopy and electron diffraction.

B. Electron energy-loss spectroscopy

The electronic structure and bonding of AlV_2O_4 were studied using electron energy-loss spectroscopy in transmission mode.^{11,12} Here, the energy lost by an electron transmitted through the sample is measured. In the single-electron approach, the excitation process can be understood as an electron in the initial state $|\Psi_i\rangle$ absorbing energy from the incident electron, and thereby being excited into an empty state $|\Psi_f\rangle$ above the Fermi level. The excitation process therefore probes the conduction band of the material. The inelastic-scattering cross section σ at an energy loss E can be described in the single-electron approximation using the Fermi golden rule:^{13,14}

$$\frac{d^2\sigma(E, \mathbf{q})}{dE d\mathbf{q}} = \frac{4\gamma^2}{a_0^2 \mathbf{q}^4} \rho(E_i + E) |\langle \Psi_f | e^{i\mathbf{q}\cdot\mathbf{r}} | \Psi_i \rangle|^2. \quad (1)$$

Here \mathbf{q} is the scattering vector determined by the experimental setup, \mathbf{r} is the position of the scattering event, a_0 is the Bohr radius, γ is the relativistic correction factor, and E_i is the energy of the electron in the initial state. The energy E lost by the incident electron corresponds to the difference in the energy of the final and initial states $E_f - E_i$, and $\rho(E_i + E)$ is the density of empty states [conduction density of states (DOS)]. For small values of \mathbf{q} the dipole approximation is valid, in which case the EELS experiment probes the atom-specific symmetry-projected DOS above the Fermi level.¹³

In the present work, we study the vanadium L edges which are caused by transitions of the type $2p \rightarrow 3d$. These

transitions therefore probe the density of empty $3d$ states. The integrated intensity of the L edges has previously been used to monitor charge transfer effects,^{15,16} while the ratio of the L_3 to L_2 intensity can furthermore be used to determine the formal oxidation state of transition metals.^{12,17–19} We also investigate the oxygen $1s \rightarrow 2p$ transitions (K edge), which probes the density of empty $2p$ states. The spectra were obtained from areas 10–50 nm in diameter, and therefore reflect an average over many unit cells.

The experiments were performed in a JEOL 2010F microscope fitted with a Gatan imaging filter (GIF200), and the Zeiss SESAM instrument at the Max Planck Institute (MPI) in Stuttgart. The SESAM instrument is equipped with a monochromator of the electrostatic Omega type and an in-column MANDOLINE energy filter.²⁰ Both instruments were operated at 200 kV, and the energy resolution was approximately 1.2 eV on the 2010F and 0.3 eV on the SESAM. Experiments were performed on both the low-temperature trigonal phase and the high-temperature cubic phase. Only small differences were observed across the phase transition, and unless otherwise stated the data presented here were obtained from the trigonal phase.

C. Real-space multiple-scattering calculations

Electron energy-loss spectra were calculated using the real-space multiple-scattering code FEFF8.²¹ Self-consistent muffin-tin potentials were obtained for spherical clusters of 99 atoms using Hedin-Lundqvist (local density approximation) self-energies.²² For the full multiple-scattering (FMS) calculations, we tested clusters containing up to 700 atoms. However, it was found that the calculations converged for clusters as small as 300 atoms. The spectra and density-of-state calculations presented here were all modeled for 357 atoms in the FMS cluster. Simulations of the oxygen K edge were performed both with and without a core hole in the $1s$ orbital. The calculations performed using a core hole were more successful in reproducing the initial shape of the spectra, and these calculations are used throughout the paper. Although the Fermi-level and final-state energies are found in the self-consistent-field calculations, FEFF8 has no means of determining the initial-state binding energies, apart from assuming that they are equal to the free-atom values. Therefore, the calculated spectra were aligned in energy to the experimental spectra.

D. Density functional theory

Density functional theory calculations of the electronic structure were performed in VASP,^{23,24} with the Perdew-Burke-Ernzerhof²⁵ exchange-correlation functionals in the generalized gradient approximation. An energy cutoff of 650 eV and a Γ -centered k -point sampling of $8 \times 8 \times 8$ (cubic) and $8 \times 8 \times 1$ (trigonal) were sufficient to converge the total energies within a few meV. The experimental lattice parameters were used throughout this study. The total energy of the trigonal phase was calculated to be -8.309 eV/atom for the trigonal and -8.234 eV/atom for the cubic phase. This confirms the fact that the trigonal phase is the more stable at lower temperatures.

Qualitative analyses of the charge transfer and bonding were performed using the electron density difference (EDD) between the unbonded procrystal, and the electron density calculated from DFT.²⁶ The resulting electron density then gives the redistribution caused by the interatomic bonding in the material. A quantitative measure of the charge redistribution was generated using Bader analyses,²⁷ which associate electron density with atoms by means of a zero-flux surface.

III. RESULTS AND DISCUSSION

At high temperatures (>700 K), AlV_2O_4 is a cubic spinel with the Al atoms tetrahedrally coordinated by oxygen at the A sites, while V occupies the octahedral B sites.²⁸ In a simple ionic picture, Al is trivalent, Al^{3+} , while vanadium has a fractional valence, $\text{V}^{2.5+}$. At lower temperatures, small distortions give a trigonal structure where the vanadium atoms are divided between three crystallographically inequivalent sites.⁶ This gives a charge-ordered state, where vanadium atoms at the three sites (V_1 , V_2 , and V_3) have slightly different valency. These are stacked along the $[111]$ direction of the cubic cell ($[001]$ of the hexagonal axes). See Fig. 1 for an illustration of the structure and the stacking of the different vanadium ions.

Figure 2 shows the vanadium L and oxygen K edges for the trigonal AlV_2O_4 . The compound displays sharp “white lines” of high intensity, as expected for low- Z transition metals (TMs). The oxygen K edge, however, displays a characteristic three-peaked shape with an intense prepeak with onset at 535 eV, and two main peaks at about 540 and 545 eV. The inset of Fig. 2 shows a comparison of the L_2 and L_3 edges of AlV_2O_4 with those of V_2O_3 . When normalized to the L_3 peak intensity, we clearly see that the $L_3:L_2$ ratio for AlV_2O_4 is higher than that of V_2O_3 . This indicates that the valence state

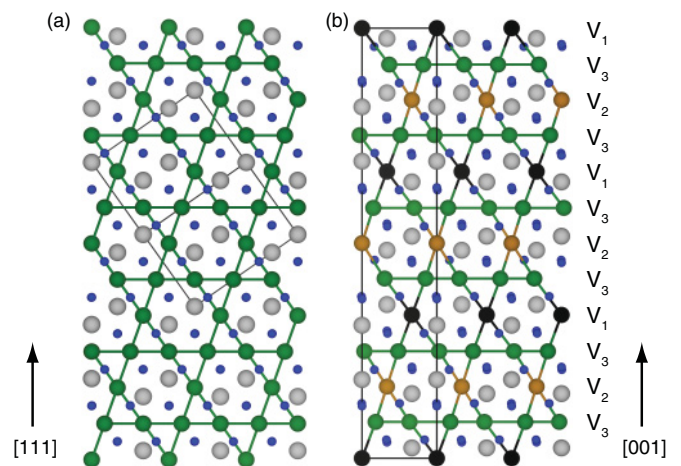


FIG. 1. (Color online) The crystal structures of the (a) cubic and (b) trigonal phases of AlV_2O_4 . The unit cell is outlined for both structures. The cubic structure is seen in the $0\bar{1}1$ projection with $[111]$ as the upward vector, while the trigonal structure is seen in the $0\bar{1}0$ projection with $[001]$ as the upward vector. The Al ions are gray and the oxygen ions blue. In the cubic phase, all vanadium atoms occupy equivalent crystallographic sites and are colored green, while in the trigonal phase vanadium occupies the three inequivalent sites V_3 (green), V_2 (orange), and V_1 (black).

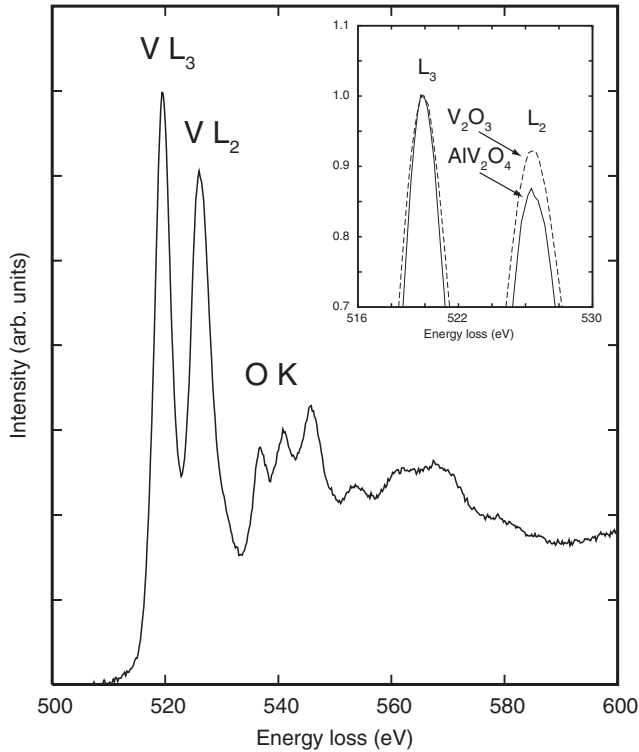


FIG. 2. The vanadium L and oxygen K edges of AlV_2O_4 . The inset is a comparison of the $L_3:L_2$ ratio of AlV_2O_4 and V_2O_3 . The comparison clearly shows a higher ratio for the AlV_2O_4 compound.

of vanadium in AlV_2O_4 is lower than in V_2O_3 (V^{3+}).¹⁸ We estimate that the increase in ratio is 6.5%, which corresponds to a change in valence from 3+ to 2.4+.²⁹ Although this deviation from the nominal valence of 2.5+ may be a real feature of the sample due to, e.g., oxygen nonstoichiometry, we estimate a total experimental uncertainty of ± 0.3 . We therefore consider the observations to be in general agreement with the simple ionic model for AlV_2O_4 with a vanadium valence of 2.5+. Experiments were performed at both high (600 °C) and low (25 °C) temperatures, and the structural transition was confirmed by observing the disappearance of the low-temperature superstructure reflections in electron diffraction. However, no significant effect of the charge ordering was observed in the spectra.

In Table I we show the DFT-calculated net charge on each ion for the low-temperature trigonal and high-temperature cubic phases of AlV_2O_4 , together with VO and V_2O_3 .

TABLE I. The net charges and magnetic moments for the low-temperature trigonal phase and high-temperature cubic phase of AlV_2O_4 . For comparison, the net charges for VO and V_2O_3 are also given.

	Trigonal		Cubic		VO	V_2O_3
	Charge	Magnetic moment	Charge	Magnetic moment	Charge	
Al_1	2.44	0	2.41	0		
Al_2	2.44	0				
V_1	1.57	2.10	1.55	1.65 to 1.71	1.31	1.66
V_2	1.49	1.11				
V_3	1.45	0.30 to 0.39				
O	-1.32 to -1.36	0	-1.38	0	-1.31	-1.10

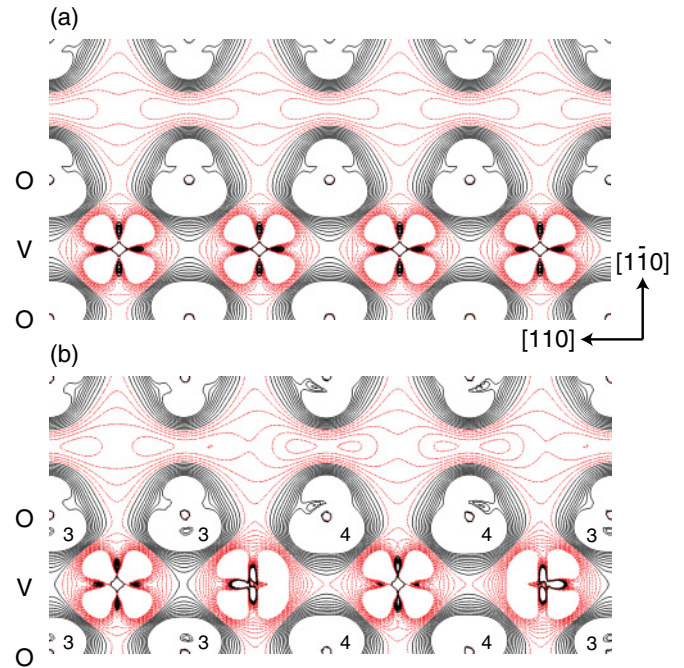


FIG. 3. (Color online) Electron density difference maps of the (a) cubic and (b) trigonal structures. The sequence of vanadium atoms is $\text{V}_2\text{-V}_3\text{-V}_1\text{-V}_3$ from left to right. In this plane, the vanadium atoms are surrounded by O_3 and O_4 atoms as indicated by the indices in the figure. The plotted densities are from $+0.02a_0^{-3}$ to $-0.02a_0^{-3}$ in steps of $0.002a_0^{-3}$, with red indicating electron depletion and black indicating accumulation.

The net charge is here defined as the nominal number of valence electrons ($\text{Al}:\text{V}:\text{O} = 3:5:6$) minus the Bader effective charge.²⁷ The net charge is then a substitute for the formal valence. Although we do not expect this calculated net charge to be directly comparable to that of the simple ionic model, trends and variations should be similar. For the trigonal phase, the net charge on the three vanadium sites varies, confirming the charge-ordering effect reported previously. The (weighted) average net charge on vanadium in the trigonal phase (+1.47) is very close to that of the cubic phase (+1.55). It is therefore not surprising that no change in valence state was observed in the experiments. However, the net charge of vanadium in AlV_2O_4 is between those of VO (+1.31) and V_2O_3 (+1.66), consistent with the experimentally observed valence state.

In Fig. 3 we give the calculated electron density difference of both the cubic and trigonal structures. Projections are

similar to the ones used in Fig. 1, but a smaller area is used for readability and only the plane containing oxygen and vanadium is shown. From this figure, we obtain qualitative information about the electron redistribution due to the setup of bonds. In the cubic case, the V-O bond length is approximately 2.04 Å. For V_1 and V_2 this remains virtually unchanged during the phase transformation. However, in the trigonal case the V_3 to O_1 and O_4 bond lengths are significantly increased to 2.10 Å, while the V_3 to O_2 and O_3 bond lengths remain close to the cubic value. A significant change in the EDD plots is therefore observed on the V_3 sites, where a clear asymmetry appears in the trigonal case due to reduced V_3 - O_1/O_4 interaction.

Close inspections of the isosurfaces reveal that the accumulation volume around oxygen extends more toward aluminum (not shown) than toward vanadium. It is therefore reasonable to assume that aluminum transfers more electrons than vanadium (i.e., the integral of this volume). Furthermore, due to the redistribution of orbitals and transfer of electrons to the oxygen ion, aluminum and vanadium are depleted (see Fig. 1) in close proximity to their centers and/or not toward the oxygen. Different behavior of aluminum and vanadium is expected due to the additional geometric freedom of the d states in vanadium. Orbital rearrangement is also seen on the vanadium site (i.e., accumulation close to its center). However, oxygen is clearly the only electron acceptor and there is no clear covalency in this structure, and it is therefore reasonable to accept all elements as contributors to the ionic bonds.

The oxygen K edge has an onset at about 535 eV, and displays a characteristic three-peaked edge shape within 15 eV of the onset. These features are unique in that none of the binary vanadium oxides display similar features, despite similar structural properties (octahedral coordination of V). However, a similar sharp intense initial peak was observed in the charge- and orbital-ordered compound $\text{Pr}_{0.5}\text{Ca}_{0.5}\text{MnO}_3$.³⁰

The oxygen K edge is caused by transitions of the type $O 1s \rightarrow 2p$ and therefore reflects the density of $2p$ states above the Fermi level. In Fig. 4 we show a closeup of the observed $O K$ edge together with a simulated spectrum and the $2p$ DOS calculated using the RSMS method as implemented in FEFF8.5 for both the cubic and trigonal structures. We note that the simulated FEFF spectrum fails to reproduce the observed peaks because of an inaccurate representation of the density of states. Peak B is not sufficiently split from A , while peak C is about 2 eV lower in energy than the experimental value.

There are several possible explanations for these discrepancies. For compounds with strong directional bonds, the spherically symmetric muffin-tin potentials may not be appropriate. Furthermore, the calculations are reliant on using a real-space cluster of sufficient size, both for the multiple-scattering calculations and for the self-consistent-field calculations. Although the spectra presented here were well converged with regard to the cluster size, newer implementations of the RSMS approach in the FEFF9 code that allow calculations with periodic boundary conditions may improve this further.³¹

The RSMS calculations are performed in the local density approximation, and also do not account for spin polarization. Although the oxygen K edge reflects the $O 2p$ DOS, spin and magnetic interactions between the $3d$ states of vanadium may play a role in determining the shape of the edge. In general, the $O 2p$ states of the transition metal oxides are strongly

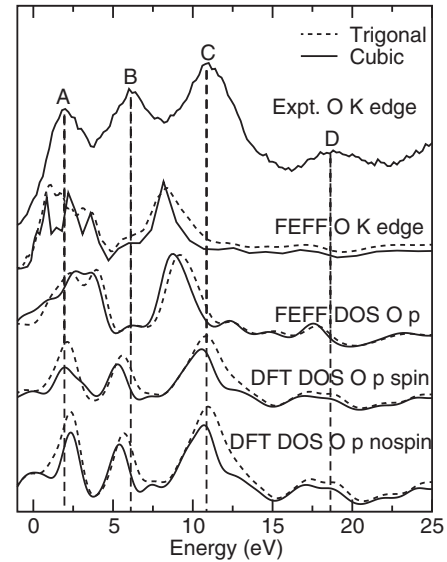
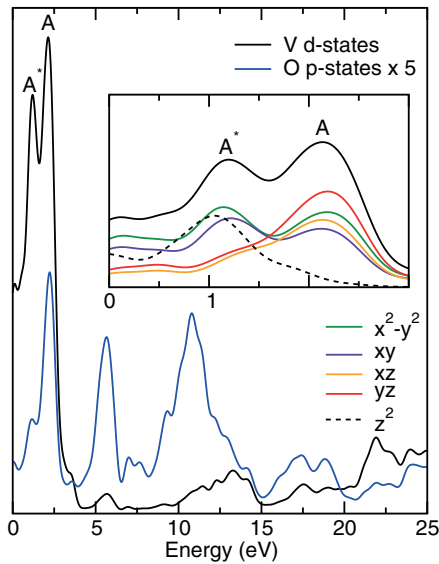


FIG. 4. Experimental $O K$ edge (top) with four peaks designated A , B , C , and D . Calculated $O K$ edge (second set from top) and $O p$ state DOS (third set from top) from FEFF. Spin-polarized (fourth set from top) and spin-restricted (fifth set from top) density functional calculations of the $O p$ states in the conduction band for both the cubic (fully drawn line) and the trigonal (dashed) structures.

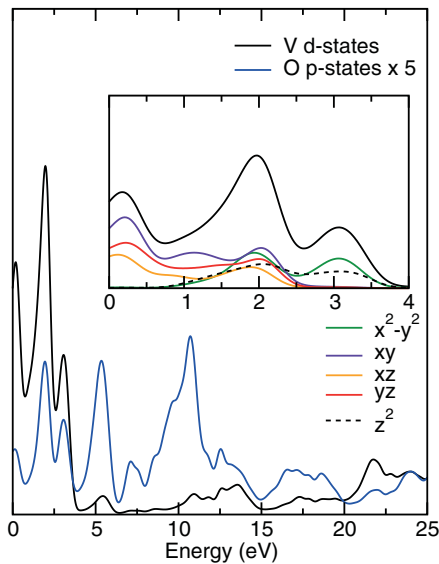
hybridized with the TM $3d$ states, and in effect the energy-loss process can be described as an $O 1s$ electron being excited into hybridized $2p$ - $3d$ states.³² The $O K$ edge may therefore be sensitive to the TM $3d$ states, and correct handling of any magnetic interactions may become particularly important. For example, Eustace and co-workers⁴ found that a correct description of magnetic interactions was essential to model the $O K$ edges of a series of chromite spinels. We should therefore investigate whether these interactions are of similar importance in the case of AlV_2O_4 .

Figure 4 shows the DFT-calculated oxygen $2p$ states, both with and without spin polarization for the cubic and trigonal structures. The three peaks in the $2p$ density of states are fully separated in all cases, giving good agreement with the experiments. Only small differences are observed for the different structures and for the calculations with and without spin interactions. It is therefore not likely that the magnetic interactions play a significant role in determining the electronic structure of this compound. The failure of the RSMS calculations is more likely caused by the inability to correctly describe the strong directional bonding of the compound.

Figure 5 shows the DOS for the oxygen $2p$ and vanadium $3d$ states from the calculations that include spin polarization for both structures. For all the peaks in the $O 2p$ states there is significant contribution from the vanadium $3d$ states. In particular, the first peak in the EELS spectrum (A) is caused by the transition into a strongly hybridized $2p$ - $3d$ state. We also note the presence of a large peak in the $3d$ DOS (marked A^*) at slightly lower energy which only weakly interacts with the oxygen $2p$ states. Projection of the $3d$ states onto the hydrogenic orbitals (inset in Fig. 5) reveals that the d_{yz} and d_{xz} orbitals contribute mostly to the peak A , while the d_{z^2} orbitals almost exclusively contribute to the peak A^* . This fits



(a) Trigonal



(b) Cubic

FIG. 5. (Color online) Calculated (DFT) vanadium d states and oxygen p states (multiplied by 5) with a Gaussian smearing of 0.2 eV. For the trigonal structure, there is strong hybridization between the second vanadium peak and the oxygen p states for the hexagonal structure. The inset shows the decomposed d orbitals of the vanadium d states.

well with the geometry and direction of the vanadium-oxygen bonds in the trigonal structure and the fact that the orbitals that are exclusively hybridized with A should be most sensitive to the vanadium-oxygen bonds. For the cubic structure, the vanadium $3d$ peak is further separated into three peaks.

A qualitative view of the magnetization of both structures is given in Fig. 6, where the density for spin-up minus spin-down electrons is plotted. Here, the difference between the two structures is substantial, and the change of magnetization between the vanadium sites is clearly visible. The magnetization of both structures was also calculated and is listed in Table I. In the cubic structure, the magnetic moments of the vanadium atoms are similar, as expected from the lattice site

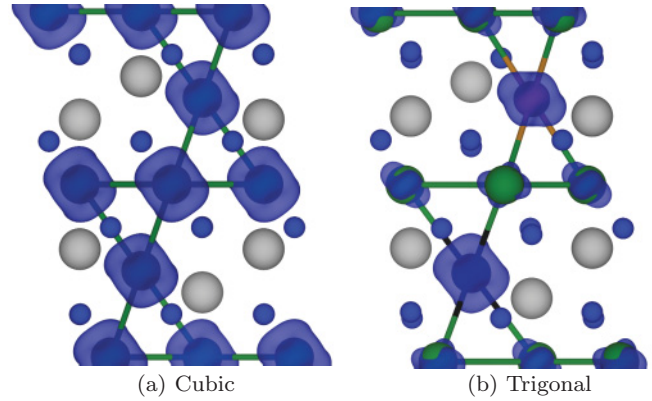


FIG. 6. (Color online) The density of spin-up minus spin-down electrons. This is analogous to the magnetization. The isosurface is set at $0.017 \mu_B/\text{\AA}^3$. Blue is positive. The negative values are significantly smaller and thus not visible at this cutoff. There is a clear difference between the cubic (a) and trigonal (b) structures.

symmetry. In the trigonal structure, however, the vanadium atoms are split between three symmetry-inequivalent sites, and the calculated magnetic moments are different. The V_1 and V_2 atoms carry rather large magnetic moments of $2.1 \mu_B$ and $1.1 \mu_B$, respectively, while for V_3 the magnetic moment is closer to zero. This is in agreement with the recent DFT study by Cai and co-workers,¹⁰ but contradicts the work by Yaresko *et al.* that found strong antiferromagnetic coupling between the vanadium sites in a study using the local spin density approximation $+U$.⁹

IV. CONCLUSIONS

In this work we combined experimental EELS measurements, real-space multiple-scattering calculations, and density functional theory to investigate the charge-ordered spinel AlV_2O_4 . The agreement between the experimental EELS spectra and the DFT-calculated O p states was surprisingly good, given the complexity of these compounds and sensitivity to the electron localization. Unfortunately, this was not the case for the real-space multiple-scattering calculations performed using FEFF8. Even though the RSMS approach has previously been useful in interpreting experimental results,^{33,34} we believe that the lack of proper description of the nonspherical contribution to the orbitals gives it limited applicability for complex oxides.

Furthermore, through the combination of DFT calculations and EELS experiments we confirmed the different charge and magnetic ordering on the vanadium and oxygen sites previously reported in the literature⁶ and also showed that the average vanadium oxidation state is approximately 2.4+.

ACKNOWLEDGMENTS

We acknowledge support from the Norwegian Research Council and the European Union under the Framework 6 program under the Contract for an Integrated Infrastructure Initiative No. 026019 ESTEEM.

- ¹R. F. Klie, Y. Zhao, G. Yang, and Y. Zhu, *Micron* **39**, 723 (2008).
- ²Y. Q. Wang, I. Maclaren, X. F. Duan, Z. H. Wang, and B. G. Shen, *J. Appl. Phys.* **90**, 488 (2001).
- ³S. Brück, M. Paul, H. Tian, A. Müller, D. Kufer, C. Praetorius, K. Fauth, P. Audehm, E. Goering, J. Verbeeck, G. Van Tendeloo, M. Sing, and R. Claessen, *Appl. Phys. Lett.* **100**, 081603 (2010).
- ⁴D. A. Eustace, D. W. McComb, and A. J. Craven, *Micron* **41**, 547 (2010).
- ⁵N. Adelstein, B. S. Mun, H. L. Ray, P. N. Ross, J. B. Neaton, and L. C. De Jonghe, *Phys. Rev. B* **83**, 205104 (2011).
- ⁶Y. Horibe, M. Shingu, K. Kurushima, H. Ishibashi, N. Ikeda, K. Kato, Y. Motome, N. Furukawa, S. Mori, and T. Katsufuji, *Phys. Rev. Lett.* **96**, 086406 (2006).
- ⁷K. Matsuno, T. Katsufuji, S. Mori, M. Nohara, A. Machida, Y. Moritomo, K. Kato, E. Nishibori, M. Takata, M. Sakata *et al.*, *Phys. Rev. Lett.* **90**, 096404 (2003).
- ⁸Y. Horibe, K. Kurushima, S. Mori, T. Asada, Y. Koyama, M. Shingu, and T. Katsufuji, *Phys. Rev. B* **71**, 052411 (2005).
- ⁹A. Yaresko, I. Leonov, and P. Fulde, *Physica B* **378–380**, 1054 (2006).
- ¹⁰Y. Cai, Z. F. Huang, X. Ming, C. Wang, and G. Chen, *J. Alloys Compd.* **505**, L23 (2010).
- ¹¹J. Taftø and J. Zhu, *Ultramicroscopy* **9**, 349 (1982).
- ¹²R. D. Leapman, L. A. Grunes, and P. L. Fejes, *Phys. Rev. B* **26**, 614 (1982).
- ¹³V. J. Keast, A. J. Scott, R. Brydson, D. B. Williams, and J. Bruley, *J. Microsc.* **203**, 135 (2001).
- ¹⁴P. Rez, in *Transmission Electron Energy Loss Spectrometry in Materials Science and the EELS Atlas*, edited by C. C. Ahn, Chap. 4 (Wiley-VCH, Weinheim, 2004), pp. 97–126.
- ¹⁵D. H. Pearson, C. C. Ahn, and B. Fultz, *Phys. Rev. B* **47**, 8471 (1993).
- ¹⁶Ø. Prytz, J. Taftø, C. C. Ahn, and B. Fultz, *Phys. Rev. B* **75**, 125109 (2007).
- ¹⁷R. D. Leapman and L. A. Grunes, *Phys. Rev. Lett.* **45**, 397 (1980).
- ¹⁸X. W. Lin, Y. Y. Wang, V. P. Dravid, P. M. Michalakos, and M. C. Kung, *Phys. Rev. B* **47**, 3477 (1993).
- ¹⁹P. A. van Aken, B. Liebsher, and V. J. Styrsa, *Phys. Chem. Miner.* **25**, 323 (1998).
- ²⁰E. Essers, G. Benner, T. Mandler, S. Meyer, D. Mittmann, M. Schnell, and R. Höschel, *Ultramicroscopy* **110**, 971 (2010).
- ²¹A. L. Ankudinov, B. Ravel, J. J. Rehr, and S. D. Conradson, *Phys. Rev. B* **58**, 7565 (1998).
- ²²L. Hedin and B. I. Lundqvist, *J. Phys. C* **4**, 2064 (1971).
- ²³G. Kresse and J. Hafner, *Phys. Rev. B* **47**, 558R (1993).
- ²⁴G. Kresse and J. Hafner, *Phys. Rev. B* **49**, 14251 (1994).
- ²⁵G. Kresse and D. Joubert, *Phys. Rev. B* **59**, 1758 (1999).
- ²⁶E. Flage-Larsen, O. M. Løvvik, Ø. Prytz, and J. Taftø, *Comput. Mater. Sci.* **47**, 752 (2010).
- ²⁷W. Tang, E. Sanville, and G. Henkelman, *J. Phys.: Condens. Matter* **21**, 084204 (2009).
- ²⁸B. Reuter, R. Aust, G. Colmann, and C. Neuwald, *Z. Anorg. Allg. Chem.* **500**, 188 (1983).
- ²⁹M. Chi, T. Mizoguchi, L. W. Martin, R. Ramesh, and N. Browning, *Microsc. Microanal.* **13**, 1234 (2007).
- ³⁰L. Wu, R. F. Klie, Y. Zhu, and C. Jooss, *Phys. Rev. B* **76**, 174210 (2007).
- ³¹K. Jorissen and J. J. Rehr, *Phys. Rev. B* **81**, 245124 (2010).
- ³²L. A. Grunes, R. D. Leapman, C. N. Wilker, R. Hoffmann, and A. B. Kunz, *Phys. Rev. B* **25**, 7157 (1982).
- ³³Ø. Prytz, R. Sæterli, O. M. Løvvik, and J. Taftø, *Micron* **39**, 685 (2008).
- ³⁴R. Sæterli, E. Flage-Larsen, Ø. Prytz, J. Taftø, K. Marthinsen, and R. Holmestad, *Phys. Rev. B* **80**, 075109 (2009).